Journal of Advanced Joining Processes 13 (2026) 100383

Contents lists available at ScienceDirect

Journal of Advanced Joining Processes

journal homepage: www.sciencedirect.com/journal/journal-of-advanced-joining-processes

Assessment of the contact parameter influence on fatigue-induced wear in clinched joints

Malte Christian Schlichter *, Jean-Patrick Ludwig, Mathias Bobbert, Gerson Meschut

Laboratory for Material and Joining Technology (LWF), Paderborn University, Pohlweg 47-49, 33098 Paderborn, Germany

ARTICLE INFO

Keywords:
Fatigue
Wear
Mechanical joining
Sheet metal
Fretting

ABSTRACT

The growing demand for lightweight body-in-white concepts, driven by stringent emission regulations, has intensified the application of mechanical joining technologies in automotive engineering. Clinching has proven to be an efficient method for joining similar and dissimilar sheet materials. However, under cyclic loading, complex wear mechanisms such as abrasion and fretting can occur, significantly affecting fatigue performance and service life. To investigate these mechanisms under realistic conditions, a novel tribo-torsion test rig was developed and validated. This setup enables the controlled reproduction of service-relevant interface pressures and relative displacements in clinched joints. A Design of Experiments (DoE) approach was applied, with test parameters derived from cyclic shear–tensile simulations at a load ratio of $R = 0.1$. The developed axial compression–torsion fretting test configuration allows high interface pressures combined with defined, cyclic displacements, capturing the transition from mild oxidative to adhesion-dominated, severe wear. These transitions are characterised by black debris formation, cold welding, and an increase in surface roughness at elevated load levels. To confirm transferability, the experimental results were benchmarked against real clinched joints under cyclic shear–tensile loading, showing strong agreement within interface pressures of 150–200 MPa and relative displacements of 130–260 µm. Furthermore, the observed roughness evolution, oxide formation, and fretting-specific debris confirmed the validity of the approach. The presented methodology thus provides a validated experimental framework for analysing tribological degradation mechanisms in clinched joints, and establishes a foundation for predictive models aimed at improving fatigue life assessment.

Introduction

Due to stricter EU environmental regulations and increasing customer demands, the automotive industry must reduce greenhouse gas emissions across vehicle fleets. A promising solution is the use of lightweight, multi-material structures, the optimised material usage leading to lower vehicle weight, thereby improving efficiency and cutting emissions (European Union 2025). In this regard, aluminium, high-strength steels, fibre composites and other lightweight materials are used, especially for body in white structures, based on their low weight, higher strength and corrosion resistance (Yan and Xu, 2025). Due to the varying materials and chemical properties of lightweight materials used today, mechanical joints have been developed to overcome limitations in joinability resulting from interfacial reactions, corrosion effects and thermal mismatch. An efficient joining process for multi-material structures made from sheet metals is clinching.

The clinching process is a widely used mechanical joining method for joining two or more sheet metals without the use of any auxiliary elements. A mechanical interlock is formed through the use of a punch-die combination by cold forming the sheets. The process is supported by a blank holder device to prevent slippage. This simple one-step process is one advantage of clinch joining, as well as the high fatigue strength of the formed joints (Deutscher, 2021). The geometrical characteristics of clinched joints are usually assessed by the neck thickness, interlock and residual bottom thickness. For static loads, clinched joints exhibit four distinct failure modes. These modes can be described as neck fracture, unbuttoning, and two mixed modes (Deutscher, 2021). However, under cyclic loading, complex wear mechanisms such as abrasion and fretting occur, significantly affecting fatigue performance and accounting for up to 90 % of service failures (Campbell, 2008).

Research into the fatigue failure of mechanical joints has seen a marked increase in recent years, with a particular focus on fracture

* Corresponding author.
E-mail addresses: amalte.schlichter@lwf.uni-paderborn.de (M.C. Schlichter), bjean.patrick.ludwig@lwf.uni-paderborn.de (J.-P. Ludwig), cmathias.bobbert@lwf.uni-paderborn.de (M. Bobbert), dmeschut@lwf.uni-paderborn.de (G. Meschut).

https://doi.org/10.1016/j.jajp.2026.100383

Available online 13 February 2026

mechanisms, such as those found in clinched or riveted joints. For clinched joints, four typical fatigue failure modes are observed: button neck fracture mode, upper-sheet separation mode, lower-sheet separation mode, and button separation or pull-out failure mode, as shown by Zhang et al. (Zhang, 2018). Mostly, the first three failure modes are investigated due to their significance. Recent studies have proven that fretting wear is another key factor influencing the fatigue life and failure of mechanical joints (Coppieters et al., 2017).

Fretting can be described as a specific form of surface degradation that arises under cyclic loading conditions. It is caused by microscale relative motion between contacting surfaces, typically within overlapping or interlocking regions of the joint. This localised movement promotes the formation of abrasive debris and oxide layers (black chips), which in turn intensify material removal and facilitate crack initiation. Fretting damage is categorised in three phases. In the initial phase, the oxide layer on the contact surfaces is removed due to mechanical wear. After this layer is completely worn away, the base material of the components is exposed, enabling adhesive interactions. This leads to the formation of micro-welds and an increase in the coefficient of friction. With continued cyclic loading, these micro-welds rupture, resulting in the generation of wear debris (Croccolo et al., 2022).

In fatigue testing of mechanically fastened or clinched joints, fretting has been recognized as a key damage mechanism, as shown by Lei et al., who added a thin copper foam layer to the joint to enhance fretting visibility and reduce fretting wear (Lei et al., 2019). Carboni et al. identified fretting at the contact interface near the base and neck of the clinch points as the primary origin of fatigue cracks in tensile-shear loaded clinched joints. FEM analyses confirmed these regions as critical fretting zones due to high stress concentrations and local micro-movements (Carboni et al., 2006). Lin et al. (Su et al., 2015) demonstrated that fretting significantly contributes to fatigue failure in both clinched and self-piercing riveted joints. Lei et al. developed a fretting fatigue damage model for titanium alloy clinched joints and validated it through experimental investigations of static strength, fatigue life, and fracture mechanisms under shear and peeling loads. Revealing that fatigue failure is primarily driven by crack initiation and propagation at specific contact regions, depending on the loading mode (Lei et al., 2025). In the study by Zhang et al., the focus was on the influence of different stress ratios on the fatigue behaviour of clinched joints, identifying a new form of inter-sheet fretting wear as a key contributor to crack initiation. Furthermore, they developed an improved fatigue life prediction model based on the Paris-Walker equation (Zhang et al., 2025). Wu et al. investigated the fretting Fatigue performance of titanium alloy under varying interface pressures to analyse the fatigue fracture and fretting wear debris. identifying a correlation between crack initiation zone depth and the fretting fatigue strength (Wu et al., 2015). Through the investigation of He et al., it was demonstrated that fretting wear not only accelerates the expansion of fatigue cracks in the joint but also influences the direction of crack propagation in the sheet metals (He et al., 2015). Schlichter et al. investigated the influence of minimal plastic deformations on the fatigue behaviour of clinched joints, showing that fretting wear was observed for all combinations and deformations (Schlichter et al., 2025). Ewenz et al. showed in an FE model the areas of high local interface pressures and relative surface motions of clinched joints. Identifying fretting wear as a failure mode for HCT590X clinched joints when exposed to specific load amplitudes (Ewenz et al., 2022). Liu et al. provided an overview of recent investigations focusing on the fatigue behaviour of clinched joints in regard to damage behaviour and fretting investigations. Showing that current research lacks a comprehensive fatigue life model that accounts for fretting-induced damage under variable loading conditions and material combinations (Liu et al., 2023).

Based on numerous studies, it can be stated that fretting fatigue is influenced by several factors, including coefficient of friction, temperature, frequency, interface pressure, relative displacement, and contact geometry, which can affect the fretting fatigue life behaviour of materials. The contact geometry is to be considered the most influential (Majzoobi and Abbasi, 2017). Iwanbuchi et al. even stated that the test rig design has an influence on the fretting formation (Iwabuchi et al., 2007). For clarity, Fig. 1 shows a simplified depiction of the tribological contact conditions relevant to this investigation.

For experimental investigation of fretting wear, various tests and testing rigs are employed. The most prominent ones include: Pin-on-disc, flat-on-flat (Di Puccio et al., 2024), ball-on-flat (Razzak et al., 2025), twin-disk rig (Britton et al., 2024), bending beam with Hertzian fretting pads (Hills and Andresen, 2021), double-lap bolted joint fretting fatigue test (Benhamena et al., 2014) and custom rigs for clinched and SPR joints (Lei et al., 2019). The newest investigations were done on the test rig of Lei et al. They used single-lap and cross-lap clinched joints to effectively isolate shear- and peel-driven fretting fatigue, revealing crack growth in the sheet overlap under shear and in the clinched neck under peel. While this enables clear load–damage correlations, the approach is limited by its idealised, uniaxial loading, which neglects multiaxial and variable-amplitude service conditions. The fixture of constraints in the cross-lap configuration distorts local stress distributions and fretting contact conditions, while fixed test frequency and environment prevent evaluation under varied service conditions (Lei et al., 2025). Zhang et al. investigated fretting wear in their studies using a self-aligning flat-on--flat torsional fretting rig with partial ring contact, allowing for a controlled comparison of fretting and sliding wear under interface pressures of up to 3.8 MPa. The test setup ensures a measurement of wear depth in the contact zone; however, it has an idealised contact geometry, introducing edge effects that do not fully replicate full contact conditions (Zhang et al., 2017).

The aim of this work is to develop a method for identifying cyclic friction wear in mechanical clinch joints. With reference to the results of Zhang et al. (Zhang et al., 2017) and Rossel et al. (Rossel et al., 2021) a new test method is being developed that enables testing of high interface pressures and low relative displacements under cyclic loading conditions. The focus is on enabling decoupled testability through various wear factors. According to the current state of research, no other test setup is capable of simulating the wear and friction behaviour that occurs in clinched joints under cyclic loading conditions. Considering the precise evaluation and simulation of cyclic wear and friction losses, it is essential to make accurate statements about the fundamental behaviour of the coefficient of friction and wear behaviour.

Experimental

Test rig and material

The experimental test conducted in the study was performed on a tribo-torsional fretting testing rig to introduce a flat-on-flat contact configuration. The testing tools and setup are schematically shown in Fig. 2. As a testing machine, an MTS Bionix 370.02 axial torsional was used with a maximum load of 25 kN, maximum torsional load of 222 Nm, and maximum torsional speed of 400 °/s, supplied by the Institute of Structural and Material Mechanics at Paderborn University. The testing frequency was set at 8 Hz for all tests based on the machine's limits and to maintain feasible test durations. The upper and lower specimens are clamped together by the testing tools and held in position via a centring pin. Through the upper tool, both the axial load and the torsional deformation are applied during the experiment. The lower tool is fixed and equipped with an internal load cell. The different interface pressures P are applied from above using a hydraulic pump.

The investigations in this study were carried out on a dual-phase steel HCT590X in a sheet thickness of 1.5 mm with a yield strength of 330 MPa and a minimum elongation A_{80} of 20 % (Salzgitter Flachstahl 2017). This dual-phase steel was selected because it is commonly used in automotive sheet metal structures.

For the experimental program, a design of experiments (DoE) approach was employed, varying interface pressure and relative motion

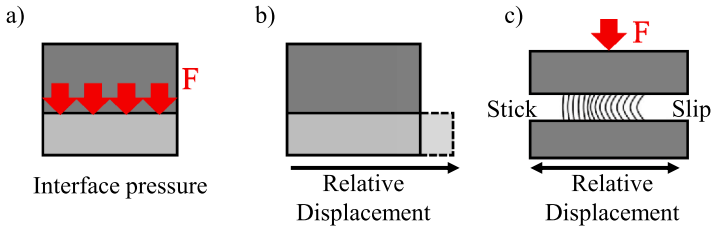

Fig. 1. Depiction of tribological contact conditions, including normal loading (interface pressure), tangential motion (relative displacement) and partial slip behaviour in partial contact.

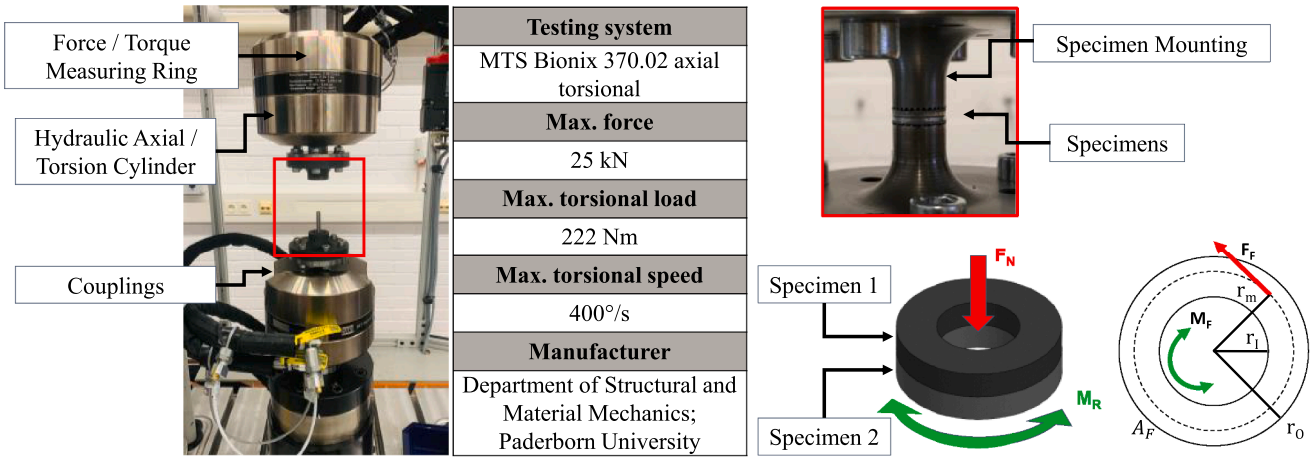

Fig. 2. Experimental test setup and specimen with depiction of the *flat-on-flat contact configuration and test mechanisms.*

as the primary factors. The parameter selection was guided by the contact conditions representative of clinched shear–tensile specimens subjected to cyclic loading with an upper load of 3.1 kN and a load ratio of $R = 0.1$. A load ratio of $R = 0.1$ was selected to reflect the shear–tensile fatigue loading commonly experienced by clinched joints in service. This maintains a non-zero minimum load, ensuring that the

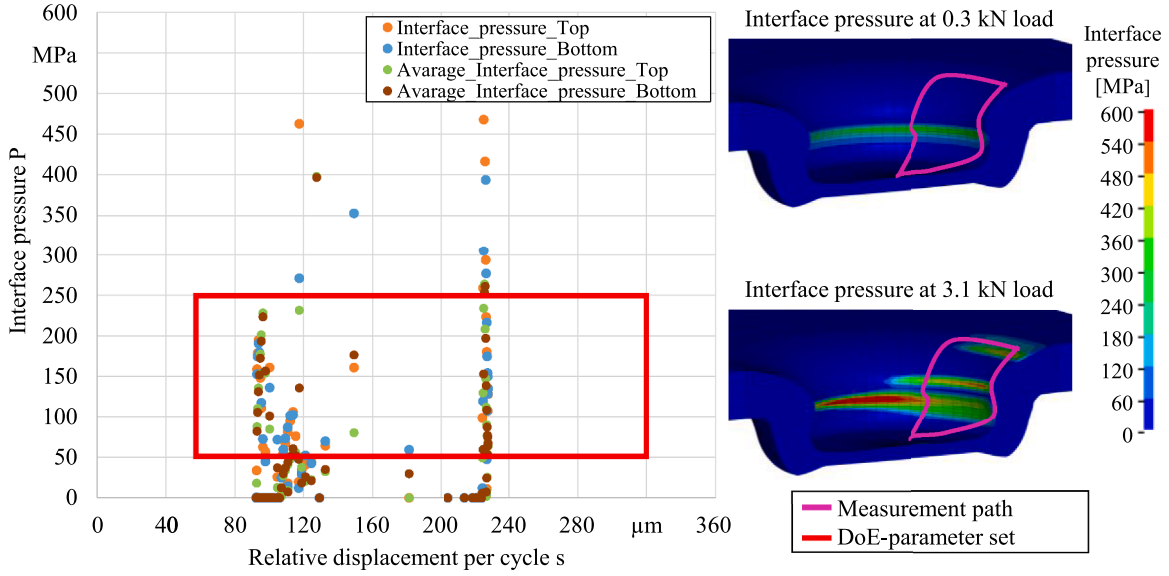

Fig. 3. Depiction of the numerical shear–tensile simulation (LS-DYNA) and resulting interface *pressures of a clinched joint under cyclic loading at a) 0.31 kN and b) 3.1 kN.*

interface remains in contact throughout the cycle. Both interface pressure and relative motion were discretised into five levels, yielding 25 parameter combinations. Each condition was tested three times to ensure statistical reliability. To replicate the relative displacements equivalent to cyclic motion in clinched joints, sinusoidal angular oscillations were applied, reproducing the kinematics of the joint under service-like conditions. The interface pressures and relative motion used in this paper are based on the shear-tensile simulation shown in Fig. 3 implemented in LS-DYNA. The simulation is based on the works of Bielak et al. (2021). To evaluate the interface pressures, the simulation was extended using the INTFOR function to determine the minima and maxima within a test cycle. Therefore, the relative displacements and interface pressure between 70 segments and 71 nodes were evaluated to determine the DoE test range.

The applied interface pressures were restricted to a maximum of 250 MPa to avoid plastic deformation, material flowing and to achieve consistent contact surfaces of the specimen during testing. All parameters, together with the effective relative displacements per cycle derived from the imposed angular amplitudes, are summarised in Table 1. The tests were conducted under controlled laboratory conditions at 23 °C and a relative humidity of 40–45 %. Each experiment was performed for 25,000 cycles. No surface preparation was carried out on the specimens prior to testing, in order to preserve realistic boundary conditions. Accordingly, the DoE levels represent discretised subsets of the simulated contact-state envelope rather than empirically chosen ranges.

Preparation of specimen and further testing methods

Due to the design of the tools used in the study, the specimens are rotationally symmetric, shaped blanks like a flat washer with a diameter of 12 mm and an inner diameter of 6 mm, as shown in Fig. 2. Due to the thin sheet metal, it is not possible to fix the specimens over the lateral surface. Therefore, force- and form-fitting mounting was achieved by utilizing a radial arrangement of grip teeth on the sheet metal surface facing away from the friction point. The specimens were produced by means of a punching process, to reduce erosion or corrosion due to cooling lubrications or water in water jet cutting or other cutting processes. Therefore, the surface conditions, friction properties, and sheet lubrication of the specimens were left untouched.

To investigate the influence of the surface wear, all specimens were weighed before and after testing on a Metteler Toledo XS205 fine scale. With a BRUKER ALICONA Infinite focus G5 optical measuring system, the surface roughness of each specimen before and after testing, as well as the effective radius r_{fric} and r_{inner}, are measured to calculate the effective radius r_{eff}. Based on this, the resulting shear stresses τ for each cycle were determined by calculating the effective friction surface (1). Since the local shear stresses fluctuate in reality during the test procedure, τ is regarded as an effective, area-averaged value in this context for comparison within the DoE. In addition, EDX and SEM measurements were taken at prominent points on the clinched joint and the blanks.

Table 1
Overview of *DoE parameters with resulting effective relative displacements per cycle.*

Design of Experiments (DoE) Parameters						
Parameter	Unit	Level 1	Level 2	Level 3	Level 4	Level 5
Interface pressure	MPa	50	100	150	200	250
Angular motion amplitudes	°	± 0.4	± 0.8	± 1.2	± 1.6	± 2.0
Effective relative displacement per cycle	µm	65	130	195	260	325

$$\tau = \frac{F_r}{A_{eff}},\ r_{eff} = \frac{2 \cdot \left(r_{fric}^3 - r_{inner}^3\right)}{3 \cdot \left(r_{fric}^2 - r_{inner}^2\right)},\ F_r = \frac{M_f}{r_{eff}} \tag{1}$$

Results and discussion

Weight loss behaviour

The weight losses of the specimens are presented in Fig. 4 as a function of interface pressure and effective relative displacement per cycle. A significant dependence of the wear behaviour on both parameters was identified, with relative displacement exerting the dominant influence. At an interface pressures of 50 MPa, the losses remain within a moderate range of 1–12 mg, with a shallow slope of the curve. This observation suggests that the contact surfaces predominantly respond elastically within this regime, resulting in only minor material removal. It was further observed that, with increasing interface pressure above 100 MPa, the variance of the results increases, resulting in overlapping. This finding indicates that, beyond this threshold, relative displacement governs the wear processes, while interface pressure assumes a secondary role. This is physically consistent with fretting theory, as the displacement amplitude controls the slip regime and thus the extent of oxide/tribofilm disruption, third-body formation and removal, and the repeated formation and rupture of adhesive junctions. By contrast, interface pressure primarily shifts the onset of these transitions and increases their severity, as evidenced by increased scatter and overlapping responses at elevated pressures. The evidence is provided by the near-linear increase in mass loss with displacement in Fig. 4 and the pronounced rise beyond 260 µm, where enhanced debris formation and adhesive/cold-welding tendencies indicate a regime change.

With increasing relative displacement, mass loss rises in an almost linear fashion. In the range of 65–195 µm (≈ 0.4–1.2 °), only moderate increases in weight loss of less than 10 mg are observed, indicating a transition from micro-slip to partial slip. Beyond 260 µm (≈ 1.6 °), however, a significant increase in weight loss is observed. This is accompanied by enhanced particle formation, marking the transition to adhesion-dominated mechanisms with pronounced material removal. The dark brown to black debris particles, “black chips,” observed under these conditions, are characteristic of oxidative abrasive wear and clearly indicate fretting.

It is notable that at a relative displacement of 325 µm (2.0 °), the maximum wear value of 23–25 mg is achieved at the applied interface pressure. In this regime, macroscopic slip occurs, accompanied by a tendency for the specimens to partially cold-weld. It has been demonstrated that this adhesion is subject to dissipation during the course of cyclic loading. Such behaviour is responsible for the pronounced fluctuations and high material losses that have been observed. This concludes that the relative displacement constitutes the primary controlling parameter of wear, whereas interface pressure predominantly influences the scatter and intensity within the transition regime.

Surface roughness development and friction contact areas

The analysis of mass loss demonstrates a noticeable dependence on both interface pressure and relative displacement. With an increase in interface pressure, there is a substantial intensification of material removal, with the most severe wear arising from the combined effect of elevated relative displacement and high interface pressure. Macroscopic examinations of all 150 specimens revealed three distinct damage phenomena (Fig. 5).

As demonstrated in Fig. 5a, 22 specimens exhibited prominent reddish-brown corrosion layers, identified by EDX analyses as zinc oxides (see Fig. 5d). These were confined to tests at 50 MPa and are attributable to oxidation of the HCT590X coating under reduced surface pressures. Under such conditions, relative displacements promote

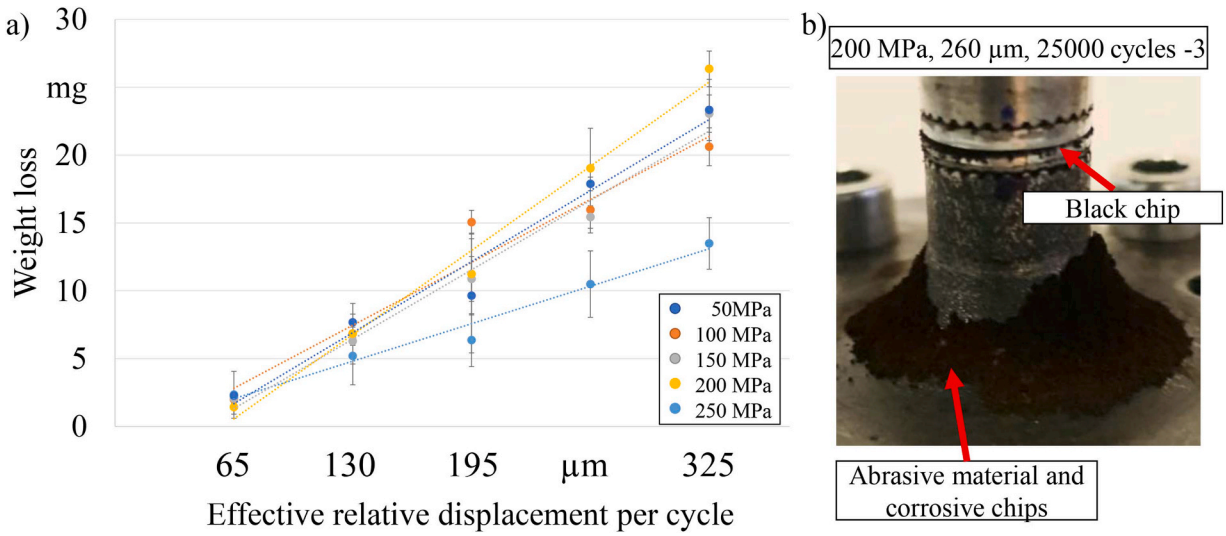

Fig. 4. Presentation of (a) weight loss based on DoE-Parameters and (b) accumulation of wear debris in axial compression–torsion testing.

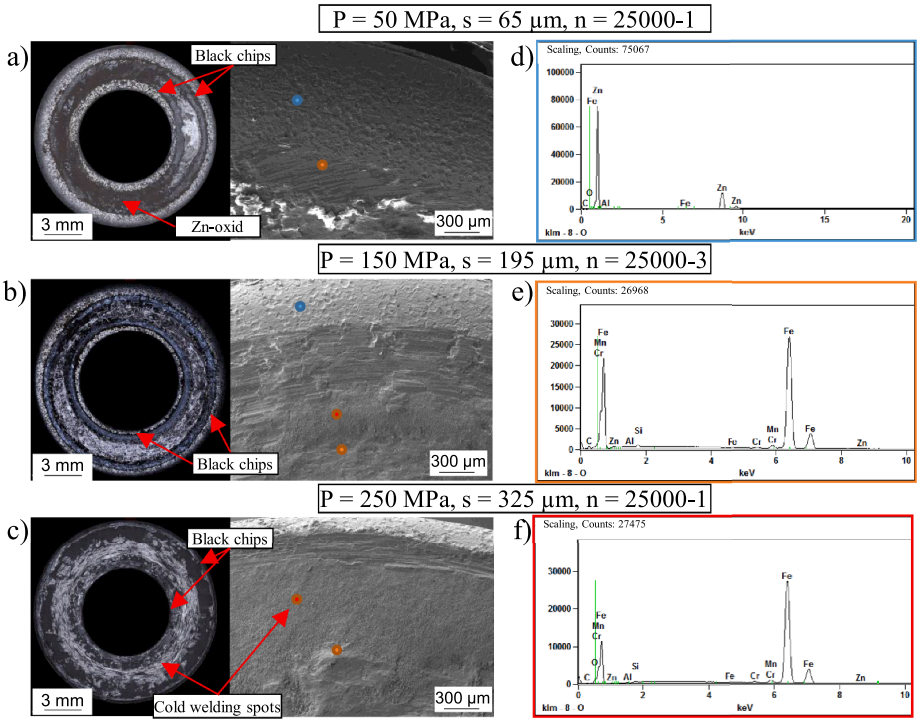

Fig. 5. Depiction of wear phenomena after axial compression–torsion testing in the form of microscopic SEM images and EDX analyses at selected surface locations.

microslip, where both abrasive and adhesive mechanisms remain limited. The inadequate expulsion of wear debris from the interface has been demonstrated to facilitate the accumulation of zinc oxides and the increase in iron concentrations, resulting in the characteristic reddish-brown colouration.

A secondary phenomenon, which was consistently observed across all specimens, was the presence of black oxide deposits at the peripheries of the effective contact areas. EDX analyses confirmed these to be iron oxide products, as indicated by elevated signals of iron and oxygen. These occurrences of black chips are markers of fretting. This hypothesis is corroborated in Carboni et al. (Carboni et al., 2006), which demonstrates that fretting is preferentially initiated at the contact peripheries where local interface pressures are reduced and microscopic relative displacements persist. In such regions, the processes of abrasion and oxidation occur concurrently, resulting in the formation of harder black chips that are characteristic of fretting. The corresponding fretting zones are highlighted in Fig. 5, together with representative EDX spectra.

Evidence of adhesive cold welding was detected at pressures exceeding 150 MPa and displacements exceeding 65 µm (1.2 °). This evidence is illustrated in Fig. 5c. This damage morphology is indicative of a transition to adhesion-dominated mechanisms with increasing load. The phenomenon of cold welding is characterised by the formation of localised solid-state bonds between the contact partners, which are periodically formed and ruptured during oscillatory motion. The formation and subsequent fracture of these solid-state bonds, resulting in a significant material removal, are illustrated in Fig. 4a. The fundamental cause of this phenomenon is the prominent increase of plastic deformation and the activation of adhesive processes, which are further

promoted by localised temperature increases at the interface. This mechanism governs the high-load regime of the experiments and significantly reduces the tribological lifetime of the specimens under constant interface pressure. The possible influence of temperature increase during testing and its resulting impact on the friction behaviour will be investigated in the future.

As illustrated in Fig. 6, the arithmetic mean roughness R_a and the maximum peak-to-valley depth R_z are influenced by cyclic surface loading. As the relative displacement per cycle increases from 65 µm to 325 µm, both roughness parameters rise markedly. The contrast between low- and high-pressure levels is particularly pronounced. As demonstrated in Fig. 6, at a pressure of 50 MPa, the roughness remains moderate even at 325 µm displacement. However, tests at 200 MPa and 250 MPa, under identical displacement, yield R_a values exceeding 15 µm and R_z values above 3 µm. Consequently, the divergence of the curves with rising load becomes more significant, suggesting a nonlinear intensification of the wear mechanism. This behaviour aligns with the classical wear theory in Archard et al. (Archard, 1953), which states that the wear rate is proportional to both the contact load and the relative motion. In this case, the wear rate is further amplified by transitions in the dominant mechanisms.

In conditions of low pressure (50 MPa), the trend lines demonstrate a flat trajectory and exhibit minimal deviation. This observation is consistent with the hypothesis that oxidic and zinc fragments from the coating act as a tribological third body, thereby shielding direct metallic contact. In this scenario, a mild oxidative wear regime prevails, which is reflected in modest roughness values and correspondingly limited mass loss. These findings are consistent with those of Baydoun et al. (Pham-Ba and Molinari, 2021), who demonstrated that sufficient oxygen supply and third-body particle formation can stabilise a mild-wear regime.

In the intermediate pressure range (100–150 MPa), the curves exhibit a significant rise, particularly for displacements exceeding 195 µm. In this regime, the protective oxide film is partially worn away, resulting in a transitional domain where oxidative abrasion and initial adhesive processes coexist. The relatively well-behaved curve trends and moderate increases in R_a and R_z are indicative of the fact that the mechanisms, although intensified, still proceed in a controlled fashion. In the extant literature, this phenomenon is frequently characterised as a transition regime, wherein mild and severe wear phenomena coexist (Pham-Ba and Molinari, 2021).

As the interface pressure increases to $\geq$ 200 MPa, a pronounced increase in the roughness, accompanied by a significant increase in deviation, becomes evident. In particular, at a relative displacement of 325 µm. Such fluctuations are characteristic of unstable adhesive processes involving localised solid-state bonds, the fracture of which leads to significant abrasion. The manifestation of these abrasions is most evidently recognizable in the precipitous rise of Rz (Fig. 6b), which describes gross surface imperfections. The values observed in this study are consistent with those reported in recent investigations of metallic contact pairs, suggesting that the wear observed here is of a severe nature (Choudhry et al., 2024).

The presence of black chips in all specimens can also be interpreted in the context of the diagrams by comparing the low- and high-pressure regimes. At 50 MPa, the relatively flat R_z values correspond to fine, oxide-dominated chips, indicating a predominantly mild wear mechanism. Conversely, at pressures ranging from 200 to 250 MPa, the R_z curves exhibit a marked increase and considerable dispersion, indicative of the presence of coarse metallic fragments. These fragments are believed to originate from the formation and rupture of bridges formed by cold welding. This qualitative change in chip morphology corroborates the trends in roughness and mass loss documented under high-pressure conditions.

When considered as a whole, the results demonstrate not only the increased surface roughness with interface pressure and relative displacement, but also substantiate the underlying transition in wear mechanisms from mild, oxide-dominated wear to unstable, adhesion-controlled severe wear. The differences between R_a and R_z, the extent of error bar scatter and the chip morphology can be consistently attributed to the governing tribological processes, in accordance with literature describing the transition from mild to severe wear (Pham-Ba and Molinari, 2021). These findings are consistent with the identified weight losses.

Investigation of shear stress evolution

The subsequent section presents exemplary shear stress data obtained from the friction tests. For the sake of clarity, the maximum shear stresses of the positive half-cycle of the relative motion are displayed. Shear stresses were calculated from the recorded torque and the effective contact area, and are plotted as peak values. The positive half-cycle was selected for analysis, as it has been demonstrated to exhibit marginally elevated shear stresses. The deviations between positive and negative half-cycles amounted to 2.7 $\pm$ 1.1 % across all tests. The methodological procedure applied for this representation is illustrated schematically in Fig. 7 for the parameter set "$P = 150$ MPa, $s = 195$ µm-2".

The shear stress evolutions depicted in Fig. 8a–e reflect the tribological behaviour as a function of interface pressure and angle-controlled relative displacement in cyclic axial compression–torsion tests. In general, the curves demonstrate a steep initial rise within the first 100 cycles, indicating a running-in phase. It has been established that, during this process, the contact surfaces undergo adaptation through plastic deformation, microslip displacements and the initial formation of wear particles. This is followed by a decline in shear stress, attributable to the early development of protective oxide layers and the transition into a quasi-stable friction regime, as demonstrated in Fig. 5a.

Subsequent phases of the tests demonstrate a corresponding rise in shear stress, accompanied by the gradual emergence of adhesion- and abrasion-dominated mechanisms. The resulting shear stress responses diverge markedly depending on the test parameters, with relative displacement exerting a pronounced influence.

At an interface pressure of 50 MPa (Fig. 8a), moderate shear stresses of 40–70 MPa are attained. For small displacements of 65–195 µm, the curves drop after the initial peak and subsequently form a plateau. In

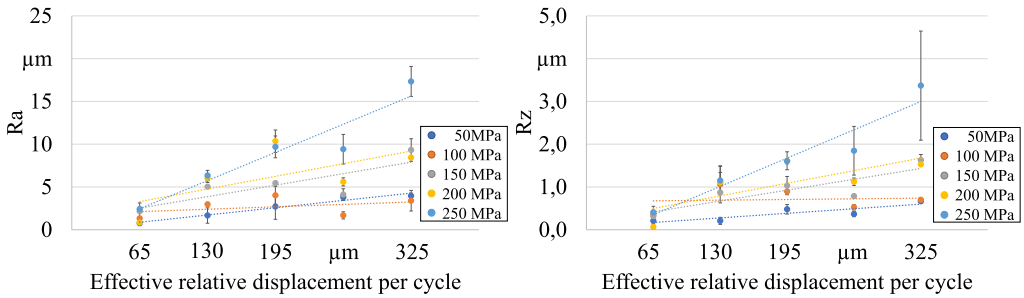

Fig. 6. Evolution of arithmetic mean roughness (R_a) and maximum peak-to-valley depth (Rz) as a function of *interface pressure and relative displacement.*

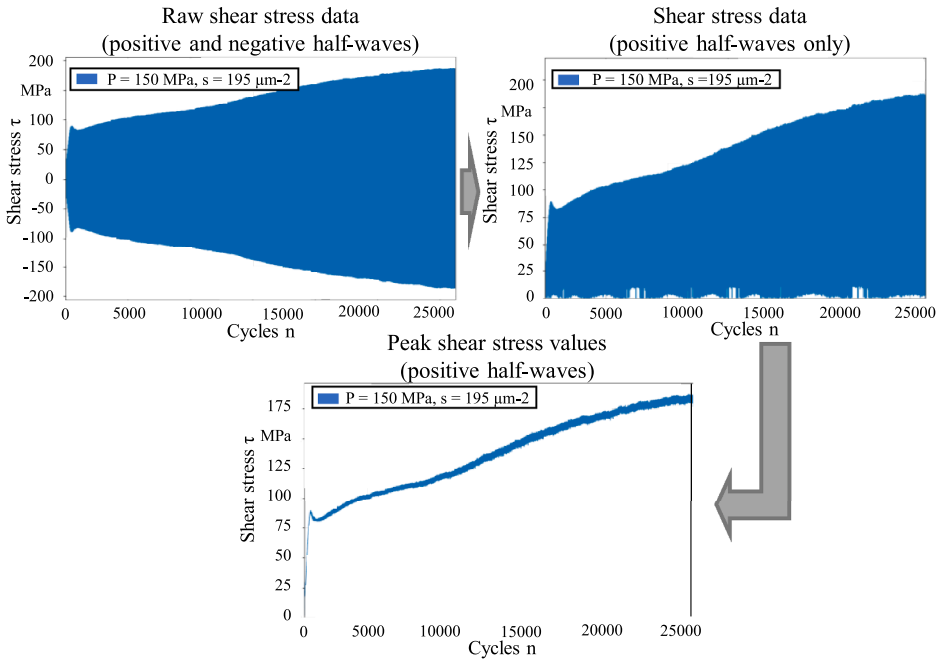

Fig. 7. Methodological representation of shear stress determination from torsional moment and effective friction area, exemplified for the parameter set "*P = 150 MPa, s = 195 µm-2*".

contrast, larger cyclic displacements exceeding 260 µm yield more stable, gradually increasing trends. This behaviour is indicative of a regime dominated by elastic deformation and mild oxidative wear mechanisms.

As the interface pressure increases to 100 MPa (Fig. 8b), the shear stress level rises substantially, to 60–140 MPa. Intermediate displacements of 195 µm exhibit a continuous increase, while smaller cyclic displacements form plateaus. Beyond 260 µm, a further increase in stress indicates the transition from a controlled elastic response to the onset of adhesive interactions. The corresponding mass losses (Fig. 4) remain dominated by elastic and mild-oxidative processes within these plateau regions. The increased occurrence of black chips at the contact peripheries confirms the initiation of oxidic–abrasive fretting wear (Baydoun and Fouvry, 2020).

With increasing pressure, from 150 MPa onwards (Fig. 8c–e), the shear stress evolution reflects a distinct transition in wear behaviour. At 65 µm, stresses stabilise after an initial peak, whereas, at larger displacements and pressures $>$ 150 MPa, they rise continuously, often exceeding 200 MPa. At $\geq$ 200 MPa and $\geq$ 260 µm, no steady state is reached; instead, strong fluctuations appear, indicating repeated cold-welding and rupture events. This behaviour marks the transition from a quasi-stable friction regime to instability, dominated by adhesive bonding and rupture. The resulting mechanisms correlate with adhesive fracture sites and pronounced roughness increases ($R_a > 15$ µm, $Rz > 3$ µm) observed on the worn surfaces (Fig. 6) (Cold welding due to impact and fretting under high vacuum, 2003).

The observed transition from mild to severe wear with increasing load agrees well with prior studies and follows Archard's wear law, in which wear volume scales with normal load and sliding distance (Archard, 1953). In the high-load regime, this relationship is amplified by adhesive mechanisms, consistent with Aghababaei et al. (2018) identifying subsurface cracking and large detachment particles under elevated pressures. These findings substantiate that the tribological response under cyclic torsion is governed not only by normal loading, but also by local adhesive fracture dynamics.

The mass-loss evolution (Fig. 4b) further supports the interpretation of shear stress behaviour. As interface pressure increases, the curves converge, demonstrating that relative displacement governs wear progression, while pressure modulates its intensity and variability. Material removal remains moderate (<10 mg) up to ≈ 195 µm, but rises sharply beyond 260 µm, accompanied by intensified debris formation and characteristic black chips (Fig. 6) as previously described by Carboni et al. (Carboni et al., 2006) and Lei et al. (Lei et al., 2025). At 325 µm, the maximum mass losses of ≈ 23–25 mg coincide with macroscopic slip and cold-welding events. This confirms that cyclic tangential displacement is the primary driver of wear progression, whereas normal pressure primarily dictates the rate of transition between mild and severe regimes.

Validation of the cyclic axial compression–torsion method on clinched joints

To assess the transferability of the disc-based axial compression–torsion tests to real-loaded clinched joints, roughness measurements and surface analytical investigations were combined. Since the disc-on-disc contact is intentionally idealised, the results are interpreted as a local contact analogue for FE-derived contact-state subsets and are used to map wear regimes to corresponding regions of the joint under cyclic shear–tensile loading. For the purpose of this investigation, forming-induced local preconditioning of the interface was not reproduced. Consequently, the following discussion focuses on mechanism and regime transferability, while quantitative values should be interpreted with this limitation in mind.

A comparison is made between the results presented and a real-loaded clinched joint that was tested for 2×10^6 cycles at an upper load of 3.1 kN. As illustrated in Fig. 8, a cross-section of the clinched joint is presented, thereby highlighting the distinctive fretting zone and unambiguously identifying black chips. The evaluation process involved executing three vertical line roughness measurements across the fretting region. The values of R_a obtained were 7.7 ± 4.3 µm, and those of R_z were 29.3 ± 13.4 µm. A comparison with the results of the specimen tests (Fig. 6a and 6b) reveals that the R_a values obtained from the torsion tests within the parameter range of 150–200 MPa and 130–260 µm fall within the corridor typically observed for actively loaded clinched joints.

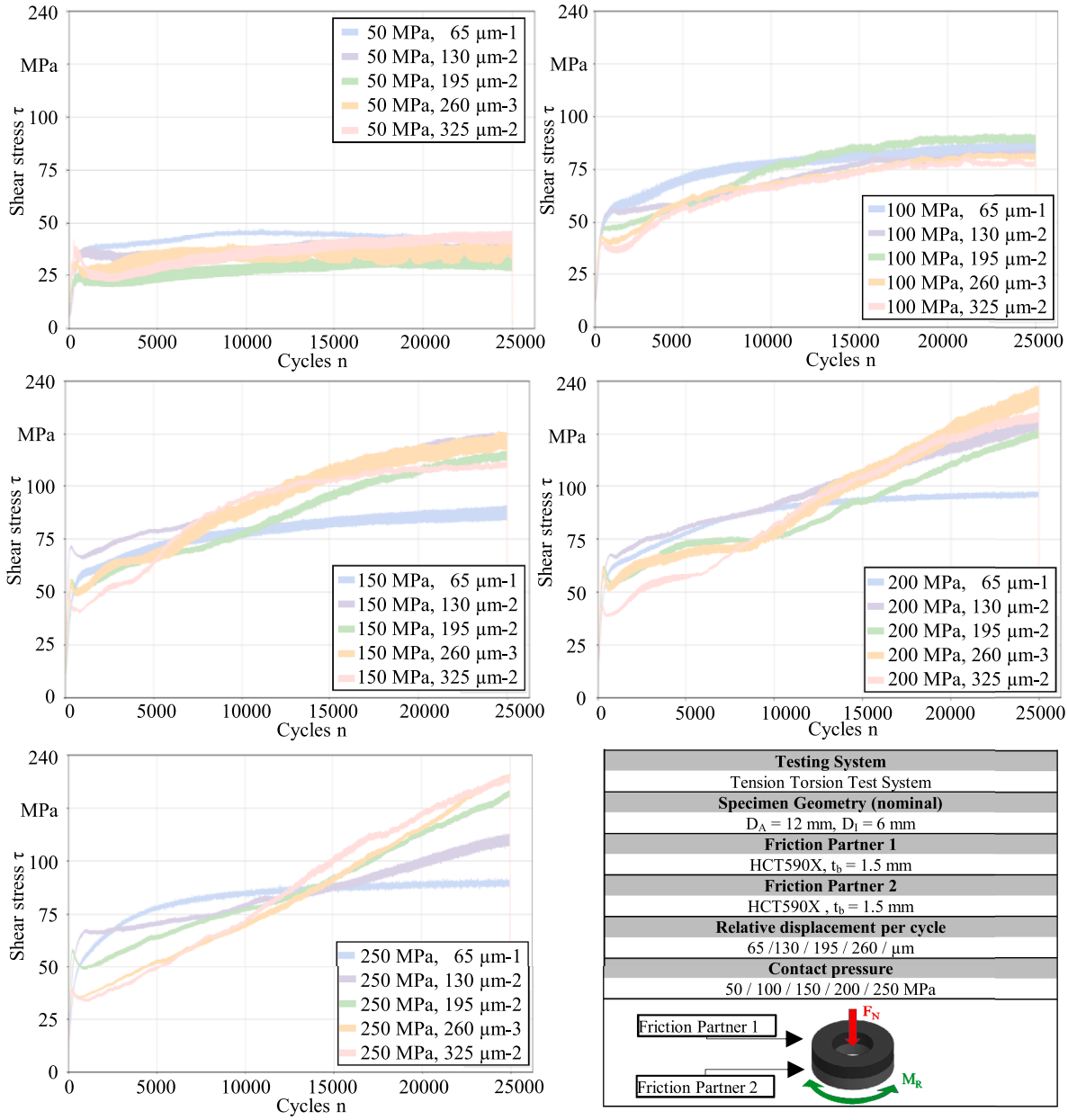

Fig. 8. Shear stress evolution in cyclic axial compression–torsion tests at varying interface pressures and angular displacements: (a) 50 MPa, (b) 100 MPa, (c) 150 MPa, (d) 200 MPa, (e) 250 MPa.

At lower loading levels, these values are frequently underestimated, whereas at high pressures and large displacements, the specimens exhibit higher levels of roughness. In contrast, the R_z values of the specimens (0.06–3.36 µm) remain well below those detected in the clinched joint (29.31 ± 13.48 µm). This discrepancy can be attributed to localised damage in the clinch joint geometry, which produces extreme roughness peaks and thus elevates the R_z level.

In addition, the peaks are located in the curvature of the joints, which makes measurements with optical metrology difficult and can lead to deflection. The underlying causes of this phenomenon are two-folded: Firstly, microcracking of the surface, and secondly, delamination of the zinc coating in the form of burrs (see Fig. 8). In contrast, the specimens exhibit a more homogeneous roughness distribution, which is attributable to the uniform contact stress distribution during testing.

According to Böhnke et al., a circular housing could be introduced to further increase the applicable interface pressure on the disc specimen (Rossel et al., 2021). Preliminary tests showed that wear debris accumulates and consolidates in the housing at high cycle numbers, which further elevates friction and can induce an unintended temperature rise. Therefore, a circular housing was not used in the present study.

A comparison of the EDX analysis for the clinched joint (Fig. 9) and the disc specimens (Fig. 5) further reveals that the zinc and oxygen signals detected in the peripheral regions of the specimens correspond well with those found in the fretting zones of the clinched joint. This finding indicates that under cyclic loading conditions, the specimens exhibit a comparable pattern of oxidic wear products (ZnO) to those observed in real-loaded clinched joints under analogous conditions. In the local area, the clinched joint displays minute Fe peaks in the neck region, denoting zinc layer breakthrough and the integration of substrate material (Fe). In contrast, the specimens exhibited a substantial increase in iron content with rising interface pressure and displacement amplitude, indicative of adhesive material transfer and localised cold

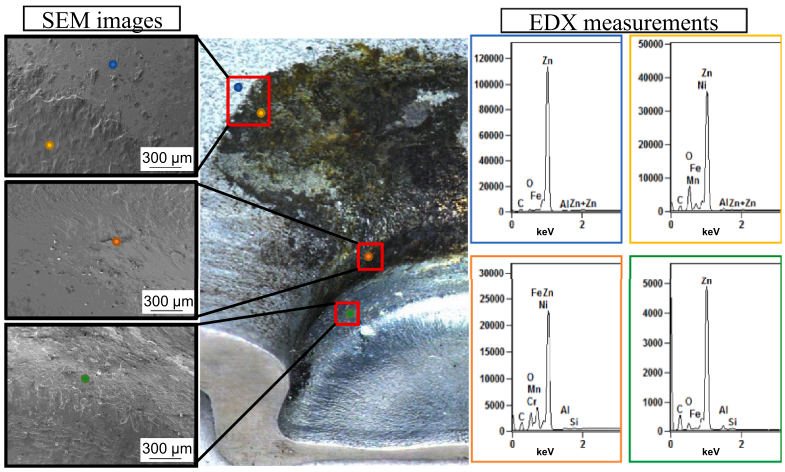

Fig. 9. Cross-section of a real clinched joint after 2×10^6 cycles at 3.1 kN, showing the distinctive fretting zone with black chips. EDX line scans reveal zinc and oxygen distributions consistent with oxidic wear products.

welding occurring in the central regions of the contact surfaces (see Fig. 5). Across all specimens, characteristic oxidic fretting-type black chips can be observed at the contact peripheries.

A comparison of the two systems provides a coherent picture of the underlying mechanisms. In both, the clinched joint and the specimen tests, oxidic products are present, indicative of mild oxidative fretting. However, distinct differences emerge in the extent of adhesive and abrasive processes. In the case of the clinched joint, these are largely confined to localised regions around microcracks and burr formations (Fig. 8), whereas in the idealised specimen contacts, more pronounced Fe signals appear under higher loads. This deviation is mechanically plausible and primarily attributable to differences in contact geometry. The parameter ranges represented in the DoE demonstrate a close parallelism with the actual contact conditions and the outcomes of fatigue tests on clinched joints, particularly within the range of 150–200 MPa at 130–260 µm. However, the axial compression–torsion test tends to overestimate real loading conditions at the boundaries of the applied DoE (see Table 1). This phenomenon can be attributed to the absence of a cyclic load ratio of $R = 0.1$, which results in an equally cyclical increase and decrease in interface pressures from a maximum load of 3.1 kN to 0.31 kN. In compression, a constantly high interface pressure is applied in the axial compression–torsion test. This identifies future parameters for fretting models that accumulate varying interfacial pressures and corresponding relative displacements during the cyclic loading of clinched joints. Future investigations will also include experiments with variable interface pressures and relative displacement profiles. Accordingly, Table 2 summarises the mapping between experimentally identified wear regimes and FE-based contact-state groups in the clinched joint.

Additionally, it identifies the dominant wear mechanisms observed in the axial compression–torsion test. Finally, it demonstrates the correspondence between these mechanisms and the findings from real clinched joints. This summary highlights the substantial consensus observed in the medium-load regime (150–200 MPa, 130–260 µm), while also emphasising the propensity of the torsion test to overemphasise the role of adhesive mechanisms under extreme boundary conditions.

The disc test's tendency to overrepresent extreme mechanisms at >200 MPa and large amplitudes is primarily due to the simplified, quasi-uniform disc-on-disc contact combined with a constant normal load. This configuration exposes a comparatively large area of the interface to sustained high compression and repeated sliding over many cycles. This promotes the formation and growth of adhesive junctions and increases the likelihood of cold-welding-type events. In real clinched joints, however, the contact is locally confined, and the interface pressure varies throughout the load cycle. This reduces the persistence of high-pressure sliding and, consequently, the probability of stable adhesive junction formation. Furthermore, near the upper boundary of the investigated parameter space, local frictional heating and changes in tribo-oxidation conditions may destabilise oxide films further and amplify adhesion in the disc test.

Table 2
Comparison of parameter ranges, dominant wear mechanisms observed in axial compression–torsion *test, and correspondence with experimentally investigated clinched joints under cyclic shear tensile loading.*

Interface pressure	Relative displacement	Dominant mechanism (disc specimens)	Comparison with clinched joints
[MPa]	**[° / µm]**	-	-
50	0.4–1.2 / 65–195	Mild oxidative wear, ZnO formation and low roughness values	Consistent with real joints: oxidic products, moderate roughness, negligible cold welding
100–150	0.4–1.2 / 65–195	Transitional regime: oxidative–abrasive processes with the onset of adhesive mechanisms	Good agreement: combination of mild and adhesive wear, black chips are detectable
150–200	0.8–1.6 / 130–260	Adhesive wear is increasingly dominant, with pronounced roughness increase, and black chips are present	Very good agreement: roughness levels, black chips, and wear mechanisms comparable to real clinched joints
>200	≥1.6 / (≥260)	Cold welding, pronounced material transfer, high roughness and scatter	Only partially observed in real joints the method tends to overrepresent extreme mechanisms

Conclusion

In summary, it has been demonstrated that the tribo-torsion method yields reproducible results, enabling the investigation of cyclic wear phenomena in sheet-to-sheet contacts of clinched joints. Within the framework of a comprehensive DoE approach, the influence of interface pressure and cyclic relative displacements under constant axial loading on wear, roughness evolution, and fretting onset could be quantitatively assessed. In comparison with alternative tribo-torsion test configurations, the present test rig facilitates the implementation of elevated interface pressures. Concurrently, it facilitates the regulated replication

of repetitive relative displacements, thus enabling a methodical examination of the predominant tribological behaviour. The results were then benchmarked against real clinched joints subjected to cyclic shear-tensile loading in order to evaluate the transferability of the method.

The interface pressure–relative displacement interaction was analysed through numerical simulation of the cyclic oscillatory behaviour of clinched joints. It has been established that, at a load of 3.1 kN, interface pressures of up to 472 MPa and relative displacements of 226 μm occur. In the present investigations, interface pressures of up to 250 MPa and displacements of up to 325 μm were studied; higher pressures could not be represented without exceeding the material yield strength during loading. The study demonstrates that the test method is well suited to characterising fretting and wear mechanisms in clinched joints. In particular, within the parameter range of 150–200 MPa interface pressure and 130–260 μm relative displacement, the roughness values, formation of black chips, and transition from mild oxidative to adhesive wear correspond closely with the findings from real clinch joints. At higher loads above 200 MPa combined with large relative displacements, pronounced cold welding and adhesive material transfer were observed phenomena not encountered to the same extent in real clinched joints. It was further identified that relative displacement exerts a significantly stronger influence on wear behaviour with increasing interface pressure.

The EDX analysis additionally confirmed the presence of identical oxidic products (ZnO, Fe-oxides) in both specimen tests and real clinched joints, thereby underscoring the relevance of the method in reproducing fretting-specific processes. The spatial manifestation of adhesive mechanisms is known to vary according to the respective contact geometries, without compromising the overall consistency of the underlying mechanisms. The findings underscore the method's remarkable sensitivity, which enables the detection of extreme wear processes and thereby expands its diagnostic capacity. Concurrently, residual overestimations must be addressed in subsequent research to facilitate a more precise analysis of cyclic wear phenomena at the elemental scale.

Lastly, the axial compression–torsion-based methodology presented here has identified a parameter space that reliably reflects the tribological conditions of real clinched joints. The method thus provides a robust approach for systematically analysing wear and friction mechanisms. Subsequent research will focus on area-resolved roughness measurements to facilitate a deeper understanding of roughness evolution. This approach will be further refined by incorporating realistic load ratios (e.g., $R = 0.1$), enabling a more comprehensive investigation of wear processes at the fundamental level. Future investigations will also include experiments with variable interface pressures and relative displacement profiles. This will ultimately provide the foundation for the development and parameterisation of a cyclically variable friction subroutine for fatigue-life modelling.

Acronyms

DoE	Design of Experiment
EDX	Energy Dispersive X-Ray Analysis
FE	Finite Element
Fe	Iron
ZnO	Zinc oxide

Funding

The authors disclosed receipt of the following financial support for the research, authorship, and publication of this article: This research was supported by the Deutsche Forschungsgemeinschaft (DFG, German Research Foundation) – TRR 285/2 – 418701707. Data regarding the contents of the publication can be requested at www.trr285.de.

CRediT authorship contribution statement

Malte Christian Schlichter: Writing – original draft, Visualization, Supervision, Methodology, Investigation, Formal analysis, Data curation, Conceptualization. **Jean-Patrick Ludwig:** Software, Methodology, Investigation. **Mathias Bobbert:** Writing – review & editing, Supervision, Project administration, Methodology, Funding acquisition, Conceptualization. **Gerson Meschut:** Writing – review & editing, Supervision, Resources, Project administration, Funding acquisition.

Declaration of competing interest

The authors declare that they have no known competing financial interests or personal relationships that could have appeared to influence the work reported in this paper.

Acknowledgments

The authors thank the German Research Foundation for their organizational and financial support. Furthermore, the authors would like to thank Prof. Dr. Richard Oswald and Dr. Ismail Caylak from the Department of Structural and Material Mechanics for providing the MTS Tension-Torsion Testing Machine and for their support during the experiments.

Data availability

Data will be made available on request.

References

Aghababaei, R., Brink, T., Molinari, J.-F., 2018. Asperity-level origins of transition from mild to severe wear. Phys. Rev. Lett. 120, 186105. https://doi.org/10.1103/PhysRevLett.120.186105.

Archard, J.F., 1953. Contact and rubbing of flat surfaces. J. Appl. Phys. 24, 981–988. https://doi.org/10.1063/1.1721448.

Baydoun, S., Fouvry, S., 2020. An experimental investigation of adhesive wear extension in fretting interface: application of the contact oxygenation concept. Tribol. Int. 147, 106266. https://doi.org/10.1016/j.triboint.2020.106266.

Benhamena, A., Aminallah, L., Baltach, A., Aid, A., Benguediab, M., Amrouche, A., Benseddiq, N., 2014. The fretting fatigue behavior of bolted assemblies. In: Öchsner, A., Altenbach, H. (Eds.), Design and Computation of Modern Engineering Materials. Springer International Publishing, Cham, pp. 187–204. https://doi.org/10.1007/978-3-319-07383-5_14.

Bielak, C., Böhnke, M., Bobbert, M., & Meschut, G. (2021). Further development of a numerical method for analyzing the load capacity of clinched joints in versatile process chains . Paper presented at ESAFORM 2021. 24th International Conference on Material Forming, Liège, Belgique. 10.25518/esaform21.4298.

Britton, W.M., Clarke, A., Evans, H.P., 2024. An experimental investigation replicating the surface behavior of ground steel gears in mixed lubrication using twin-disk testing part 2: micropitting. Tribol. Trans. 67, 1084–1101. https://doi.org/10.1080/10402004.2024.2378811.

Campbell, F.C., 2008. Elements of Metallurgy and Engineering Alloys. ASM International.

Carboni, M., Beretta, S., Monno, M., 2006. Fatigue behaviour of tensile-shear loaded clinched joints. Eng. Fract. Mech. 73, 178–190. https://doi.org/10.1016/j.engfracmech.2005.04.004.

Choudhry, J., Almqvist, A., Larsson, R., 2024. Improving Archard's wear model: an energy-based approach. Tribol. Lett. 72, 1–15. https://doi.org/10.1007/s11249-024-01888-8.

Cold welding due to impact and fretting under high vacuum; 2003.

Coppieters, S., Zhang, H., Xu, F., Vandermeiren, N., Breda, A., Debruyne, D., 2017. Process-induced bottom defects in clinch forming: simulation and effect on the structural integrity of single shear lap specimens. Mater. Des. 130, 336–348. https://doi.org/10.1016/j.matdes.2017.05.077.

Croccolo, D., de, Agostinis M, Fini, S., Olmi, G., Robusto, F., Scapecchi, C., 2022. Fretting fatigue in mechanical joints: a literature review. Lubricants 10, 53. https://doi.org/10.3390/lubricants10040053.

D.VS.-. Deutscher Verband für Schweißen und verwandte Verfahren e.V. Merkblatt DVS/EFB 3420: clinching - basics. 2021.

Di Puccio, F., Di Pietro, A., Mattei, L., 2024. Pin-on-plate vs. pin-on-disk wear tests: theoretical and numerical observations on the initial transient phase. Lubricants 12, 134. https://doi.org/10.3390/lubricants12040134.

European Union, 2025. Regulation (EU) 2025/1214 of the European Parliament and of the Council of 17 June 2025 introducing additional flexibility for the 2025–2027 compliance period under regulation (EU) 2019/631. Off. J. Eur. Union L, 1214.

Ewenz, L., Bielak, C.R., Otroshi, M., Bobbert, M., Meschut, G., Zimmermann, M., 2022. Numerical and experimental identification of fatigue crack initiation sites in clinched joints. Prod. Eng. Res. Devel. 16, 305–313. https://doi.org/10.1007/s11740-022-01124-z.

He, X., Zhao, L., Deng, C., Xing, B., Gu, F., Ball, A., 2015. Self-piercing riveting of similar and dissimilar metal sheets of aluminum alloy and copper alloy. Mater. Des. (1980-2015) 65, 923–933. https://doi.org/10.1016/j.matdes.2014.10.002.

Hills, D.A., Andresen, H.N., 2021. Experiments to Measure Fretting Fatigue Strength. In: Hills, D.A., Andresen, H.N. (Eds.), Mechanics of Fretting and Fretting Fatigue. Springer International Publishing, Cham, pp. 151–160. https://doi.org/10.1007/978-3-030-70746-0_8.

Iwabuchi, A., Lee, J.W., Uchidate, M., 2007. Synergistic effect of fretting wear and sliding wear of Co-alloy and Ti-alloy in Hanks' solution. Wear 263, 492–500. https://doi.org/10.1016/j.wear.2007.01.102.

Lei, L., He, X., Xing, B., Zhao, D., Gu, F., Ball, A., 2019. Effect of foam copper interlayer on the mechanical properties and fretting wear of sandwich clinched joints. J. Mater. Process. Technol. 274, 116285. https://doi.org/10.1016/j.jmatprotec.2019.116285.

Lei, L., Shi, Y., He, X., 2025. Fretting fatigue damage of titanium alloy clinched structure. J. Materi Eng. Perform. 34, 14746–14756. https://doi.org/10.1007/s11665-024-10183-5.

Liu, F., Chen, W., Deng, C., Guo, J., Zhang, X., Men, Y., Dong, L., 2023. Research advances in fatigue behaviour of clinched joints. Int. J. Adv. Manuf. Technol. 127, 1–21. https://doi.org/10.1007/s00170-023-11547-2.

Majzoobi, G.H., Abbasi, F., 2017. On the effect of contact geometry on fretting fatigue life under cyclic contact loading. Tribol. Lett. 65, 1–17. https://doi.org/10.1007/s11249-017-0906-9.

Pham-Ba S., Molinari J.-.F. Adhesive Wear Regimes on Rough Surfaces and Interaction of Micro-contacts; 2021.

Razzak, A., Wang, S., Xue, W., Gao, S., Duan, D., 2025. Study on fretting wear behavior of titanium alloys sliding against various friction pair materials at room temperature for aero-engine applications. J. Bio. Tribo. Corros. https://doi.org/10.1007/s40735-025-00957-2.

Rossel, M., Böhnke, M., Bielak, C.R., Bobbert, M., Meschut, G., 2021. Development of a method for the identification of friction coefficients in sheet metal materials for the numerical simulation of clinching processes. Int. Conf. Sheet Met. 883, 81–88. https://doi.org/10.4028/www.scientific.net/KEM.883.81.

Salzgitter Flachstahl, 2017. HCT590X+Z: mehrphasenstähle zum Kaltumformen – Dualphasenstähle. https://www.salzgitter-flachstahl.de/fileadmin/footage/MEDIA/gesellschaften/szfg/informationsmaterial/produktinformationen/feuerverzinkte_produkte/deu/hct590x.pdf.

Schlichter, M.C., Harabati, Ö., Böhnke, M., 2025. Investigation on manufacturing-induced pre-deformation on the fatigue behaviour of clinched joints. Sheet Met. 52, 125, 2025Materials Research Forum LLC; 2025.

Su, Z.-M., Lin, P.-C., Lai, W.-J., Pan, J., 2015. Fatigue analyses of self-piercing rivets and clinch joints in lap-shear specimens of aluminum sheets. Int. J. Fatigue 72, 53–65. https://doi.org/10.1016/j.ijfatigue.2014.09.022.

Wu, G.Q., Liu, X.L., Li, H.H., Sha, W., Huang, L.J., 2015. Effect of contact pressure on fretting fatigue behavior of Ti-1023. Wear 326-327, 20–27. https://doi.org/10.1016/j.wear.2014.12.033.

Yan, L., Xu, H., 2025. Lightweight composite materials in automotive engineering: state-of-the-art and future trends. Alex. Eng. J. 118, 1–10. https://doi.org/10.1016/j.aej.2024.12.002.

Zhang, P., Lu, W., Liu, X., Zhou, M., Zhai, W., Zhang, G., et al., 2017. Torsional fretting wear behavior of CuNiAl against 42CrMo4 under flat on flat contact. Wear 380-381, 6–14. https://doi.org/10.1016/j.wear.2017.03.002.

Zhang, Y., Peng, J., Peng, R., Lei, B., Jiang, J., 2025. Fatigue fracture mechanism and life prediction of steel-aluminium clinched joints under different stress ratios. Thin-Walled Struct. 207, 112721. https://doi.org/10.1016/j.tws.2024.112721.

Zhang, Y., 2018. Fretting fatigue mechanism research of the aluminum alloy clinched joints. JME 54, 190. https://doi.org/10.3901/jme.2018.19.190.